coatings

MDPI

Article

The Influence of Polymer Blends on Regulating Chondrogenesis

Aneel Bherwani [1], Chung-Chueh Chang [2], Gadi Pelled [3,4], Zulma Gazit [3,4], Dan Gazit [3,4], Miriam Rafailovich [2] and Marcia Simon [1,*]

1 Oral Biology and Pathology Stony Brook University, Stony Brook, NY 11794, USA
2 Materials Science and Engineering, Stony Brook University, Stony Brook, NY 11794, USA
3 Skeletal Biotech Laboratory, The Hebrew University of Jerusalem, Jerusalem 94142, Israel
4 Department of Surgery and Board of Governors Regenerative Medicine Institute, Cedars-Sinai Medical Center, Los Angeles, CA 90048, USA
* Correspondence: marcia.simon@stonybrook.edu

Received: 29 May 2019; Accepted: 15 July 2019; Published: 18 July 2019

Abstract: The influence of polymer blend coatings on the differentiation of mouse mesenchymal stem cells was investigated. Polymer blending is a common means of producing new coating materials with variable properties. Stem cell differentiation is known to be influenced by both chemical and mechanical properties of the underlying scaffold. We therefore selected to probe the response of stem cells cultured separately on two very different polymers, and then cultured on a 1:1 blend. The response to mechanical properties was probed by culturing the cells on polybutadiene (PB) films, where the film moduli was varied by adjusting film thickness. Cells adjusted their internal structure such that their moduli scaled with the PB films. These cells expressed chondrocyte markers (osterix (OSX), alkaline phosphatase (ALP), collagen X (COL-X), and aggrecan (ACAN)) without mineralizing. In contrast, cells on partially sulfonated polystyrene (PSS_{28}) deposited large amounts of hydroxyapatite and expressed differentiation markers consistent with chondrocyte hypertrophy (OSX, ALP, COL-X, but not ACAN). Cells on phase-segregated PB and PSS_{28} films differentiated identically to those on PSS_{28}, underscoring the challenges of using polymer templates for cell patterning in tissue engineering.

Keywords: polymer substrates; mesenchymal stem cells; modulus; biomineralization; chondrogenesis

1. Introduction

Controlled delivery of growth factors and cytokines has been proposed as adjunctive therapy for bone regeneration. As early as 2001, recombinant human BMP-7 was approved as a humanitarian device for treatment of nonhealing long bone fractures, and soon after, human BMP-2 (rhBMP-2) was approved for spinal fusion [1]. It has been shown that in situ, this cytokine promotes endochondral ossification, while its absence delays development of secondary ossification centers [2–7]. Off target effects at high doses may occur and include ectopic bone formation, bone resorption and soft tissue swelling [8–12]. Hence, additional treatment options for BMP-2-driven functions have been considered.

One such option is the application of mesenchymal stem cells (MSCs). These cells can undergo chondrogenesis or osteogenesis dependent upon the environmental niche. Early work carried out with a mouse embryonic MSC cell line (C3H10T1/2) demonstrated that when grown in micromass cultures chondrogenesis could be induced with BMP-2 [13]. Furthermore, in experiments using C9, a a cell line derived from C3H10T1/2 by genetically engineering to express rhBMP-2 in the absence of tetracyclines or its analogues (e.g., doxycycline), MSCs will undergo osteochondrogenesis in vitro and will support bone healing in vivo [14–17]. Although MSCs will migrate to multiple sites following intravenous

injection, they can also be applied directly to the target area either in suspension or on various scaffolds including those prepared with osteo-inductive and angiogenic-promoting factors [18–24]. It is therefore of interest to optimize scaffolds supporting MSC differentiation.

The ability of substrates to regulate differentiation has been well documented. The difference in cell response is due not only to unique substrate binding sites, but also to substrate topography and mechanics. Substrate properties can be easily controlled in the design of different polymeric materials. Here we focus on two polymers with very different surface properties, one a soft elastomer, and a second a glassy, highly charged polymer. The large differences between the polymers are expected to elicit very different responses in cell culture. The large differences between the two polymers also assures that, when blended, they will be highly immiscible and form heterogeneous scaffolds that would allow us to study the influence of surfaces presenting a combination of the surface properties.

The response of stem cells to substrate mechanics was previously documented on acrylamide gels where the cells where shown to undergo alternative differentiation paths [25–31] in response to changes in substrate moduli. In the case of hydrogels, the substrate rigidity was modulated in large increments via cross linker chemistry, and the gels were subsequently coated with collagen to enable cell adhesion. A different approach was demonstrated using dental pulp stem cells, polybutadiene (PB) [32], and partially (28%) sulfonated polystyrene (PSS_{28}). These two polymers allow for small, incremental changes in mechanical and charge properties, without additional cross linkers or cell adhesion coatings, making interpretation of the results more straightforward. Polybutadiene is a hydrophobic elastomeric polymer (glass transition, Tg < −40 °C) whose bulk modulus, M = 0.9 (0.1) MPa [33], is similar to the values previously reported for the aggregate modulus of healthy cartilage, M = 0.5–0.9 MPa [34]. When spun cast, the modulus of PB can be increased by a factor of seven for films approximately 20 nm thick [32]. Hence this polymer allows us to probe the influence of mechanics (within this range) without any other chemical modifications. Polystyrene is a glassy polyelectrolyte (Tg = 110 °C), where the charge on the polymer can be controlled by the degree of sulfonation, which in this case is 28%. Partially sulfonated styrene films have been shown to facilitate protein adsorption and induce fibrillar self-assembly of extracellular matrix (ECM) proteins [35,36]. It should be noted that only highly polymerized, high molecular weight, monodispersed versions of both PB and PSS28 are used since the monomers are toxic, and hence, despite their usefulness for in-vitro testing, these polymers are not yet available in a form that can be approved for in-vivo use (OSHA).

Using the genetically engineered mouse MSC line, C9 [15], where BMP-2 can be chemically regulated, we studied the response of the cells, first on Si wafers coated with films of PB or PSS_{28} separately, where we were able to determine that the different scaffolds had a profound influence on the cellular response to BMP-2 expression. Then we probed the ability to modulate the response in a coating composed of a 1:1 binary blend of the polymers. In addition to their very different chemical and mechanical properties, these polymers were chosen since they had a common co-solvent which enabled us to spin cast blended films. Furthermore, annealing the films produced phase-segregated morphologies with a heterogeneous surface morphology that introduced both topographical features and associated chemical heterogeneity.

2. Materials and Methods

Cell Culture: The mouse MSC line C9 was used for all experiments. This cell line was genetically engineered from C3H10T1/2 to contain recombinant human BMP2 (rhBMP2) under the control of the tetracycline response element (Tetoff®) [15]. In this cell line, the expression of rhBMP2 is suppressed by tetracycline and its analogues such as doxycycline. To expand C9, cells were plated, directly onto the polymer coated Si substrates at a density of 2000/cm^2 and cultured in "growth medium" composed of Dulbecco's Modified Eagle's Medium (DMEM) (Gibco) supplemented with 10% fetal bovine serum (FBS; Hyclone, Logan, UT, USA), 2 mM L-glutamine, 100 U mL^{-1} penicillin, 100 µg/mL streptomycin (Invitrogen, Carlsbad, CA, USA), and 1 µg/mL doxycycline (Sigma-Aldrich, St. Louis, MO, USA). For experiments testing differentiation, cells were cultured in growth medium supplemented with

10 mM β-glycerophosphate and 0.05 mM ascorbic acid-2-phosphate (Sigma-Aldrich) either without doxycycline to express rhBMP2 or with doxycycline as control. Media were changed on alternate days and cultures incubated at 37 °C, and 7% CO_2. For passage, cultures were washed with Ca^{2+}- and Mg^{2+}-free phosphate buffered saline, pH 7.4 (PBS), and incubated with 0.05% trypsin/EDTA for 10–15 min at 37 °C. Following cell detachment from the surface an equal volume of growth medium was added and cells were harvested by centrifugation.

Spin Casting: Polymer coated Si wafers used as substrates for cell plating were produced via spin coating of polymer solutions onto atomically, one side polished, flat Si wafers (RMS 0.6 nm) as follows: Polybutadiene (Mw = 205,800 and Mw/Mn = 1.49, Polymer Source, Dorval, QC, Canada) was dissolved in toluene (certified ACS and ACROS) to produce solutions at two concentrations (w/v), 3 and 20 mg/mL, which were then spun cast at 2500 rpm onto hydrofluoric (HF) acid etched [1,0,0] orientation Si wafers (Wafer World, West Palm Beach, FL, USA). The corresponding film thicknesses were measured by ellipsometry to be 20 and 200 nm. To remove residual solvent, relax spin-induced stress, and achieve sterilization, the samples were annealed in high vacuum (10^{-8} Torr) at 150 °C for 24 h.

Monodispersed, Mw/Mn < 1.1, sulfonated polystyrene, 28% sulfonation, PSS_{28} (Polymer Source, Dorval, QC, Canada), Mw = 15 kDa, were dissolved in dimethylformamide (DMF) at a concentration of 10 mg/mL and spun cast onto HF-etched Si [1,0,0] wafers to achieve a film thickness of 20 nm. To remove excess solvent and achieve sterilization, the samples were annealed in an oil-trapped vacuum oven at 10^{-4} Torr vacuum for 24 h. The polymer blend samples were produced by first dissolving the 3 mg/mL PB and 10 mg/mL PSS_{28} in toluene and DMF, then mixing the solutions in the appropriate ratios to achieve a 1:1 mass balance. The solutions were then spun cast onto HF etched Si wafers and annealed at 10^{-4} Torr, T = 170 °C, for 24 h in order for phase segregation to approach equilibrium.

Shear Modulation Force Microscopy (SMFM): Cell and substrate moduli were measured by shear modulation force microscopy (SMFM) using a Dimension 3000 scanning force microscope (Brucker/Digital Instruments, Santa Barbara, CA, USA). The experimental setup of the SMFM method was described previously [37,38]. This method uses an AFM tip (Si_2N_4 cantilever with a force constant of 0.032 N/m) to indent the surface. The tip is then laterally modulated, and the mechanical response of the substrate to the modulation is fed into a lock-in amplifier where both amplitude and phase are recorded. During the measurement, a normal indenting force of 25 nN is exerted by the cantilever to maintain contact with the surface. At the same time, a sinusoidal drive signal was applied to the x-piezo controlling the cantilever to induce a small oscillatory motion. The lateral deflection (response) amplitude (ΔX) of the cantilever is then measured and plotted against the drive amplitude. From the slopes of the response function, we can then calculate the moduli as previously described [38,39]. For each condition measurements were made of three different cells or fibers, and three points on each cell or fiber. The values quoted are the average of nine measurements with the associated errors.

Laser Scanning Confocal Microscopy (LSCM): After incubation, the cells were fixed in 3.7% formaldehyde for 15 min and rinsed with PBS three times. The samples were then permeabilized with 0.4% Triton X-100 (Sigma, St. Louis, MO, USA) and stained with Alexa Fluor® 488 Phalloidin (Invitrogen) to visualize the actin cytoskeleton. Samples were analyzed and images captured using a Leica TCS SP2 LSCM (Leica micro-systems).

Scanning Electron Microscopy and Energy Dispersive X-ray Spectroscopy (SEM/EDX): Mineral deposits were visualized using scanning electron microscopy (Zeiss, LEO1550, Oberkochen, Germany) with a 20 kV acceleration voltage and a 10 mm working distance. Samples were prepared by gently washing with deionized water to remove soluble salts from the surface and then air dried for at least 24 h. For SEM imaging, the samples were sputter-coated with gold for 15 s and loaded on aluminum stubs. The elemental compositions of deposits on the samples were imaged using energy dispersive X-ray spectroscopy in conjunction with SEM.

Quantitative Real Time-Polymerase Chain Reaction: On day 14 post-plating the cells were detached from the surface by trypsin and harvested by centrifugation as above. The cell pellet was lysed and the

RNA stabilized using the Qiagen RNeasy kit (RNeasy kit, Qiagen, Valencia, CA, USA). Total RNA (1 μg) was reverse-transcribed with 200 units Superscript II Reverse Transcriptase (Invitrogen) into cDNA using 200 ng of random primers (Invitrogen). The cDNA was used as a template in the PCR using primers for osteocalcin (OCN), alkaline phosphatase (ALP), osterix (OSX), aggrecan (ACAN), and collagen X (Col-X). 18S rRNA was used as a housekeeping gene to normalize mRNA expression. The sequences of the specific primer sets are listed in Table 1. Quantitative Real-time PCR (qRT-PCR) was performed using the SYBR Green PCR kit (Qiagen, Valencia, CA, USA) and controlled in a DNA engine MJ Opticon 2 Thermal Cycler with continuous fluorescence detection (MJ Research Incorporation, Union, NJ, USA). DNA amplifications were performed under the following conditions: 95 °C (15 min), followed by 40 cycles of 94 °C (30 s), 55 °C (30 s), and 72 °C (30 s). A melting curve was performed immediately after the above cycling program in order to generate a first derivative dissociation curve for each sample and dilution series by using the instrument's software.

Table 1. Primers used to monitor osteogenesis and chondrogenesis

rhBMP-2	Forward GACCACCGGTTGGAGAGGGCA, reverse GGTCACGGGGAATTTCGAGTTGG
OSX	forward CCTGACTCCTTGGGACCCGGTC, reverse CTGGGTAGGCGTCCCCCATGG
ALP	forward TCCTGGGAGATGGTATGGGCGTC, reverse GTTGCATCGCGTGCGCTCTG
COL-X	forward CGCATCTCCCAGCACCAGAATC, reverse GGTGTCCTCGAGGTCCGGTTG
ACAN	forward TCAACCGTTGCAGACCAGGAGCA, reverse CAGGCTGGTTTGGACGCCACT
18S	forward GTAACCCGTTGAACCCCATT, reverse CCATCCAATCGGTAGTAGCG

Statistical Analysis: All experiments were carried out in triplicate and data analyzed using a t-test with significance at $p < 0.05$. Moduli and mRNA levels are shown as the mean and standard deviation.

3. Results and Discussion

Cell Growth on PB and PSS_{28}: We first evaluated the ability of spun cast films of PB (20 and 200 nm thick) and PSS_{28} to support cell growth. Cells were incubated on each substrate for 4 days in growth medium supplemented with ascorbic acid-2-phosphate (50 μM) and β-glycerol phosphate (10 nM) with ($DOXY^+$/$rhBMP2^-$) or without ($DOXY^-$/$rhBMP2^+$) doxycycline (1 μg/mL), and then fixed and stained with Alexa Fluor® 488-phalloidin to visualize microfilaments. As we can see in Figure 1, on both the 20 nm and 200 nm PB films, cells grew well, confirming the lack of toxicity reported for the monomer in the monodispersed high Mw polymer films. Those grown with doxycycline ($DOXY^+$/$rhBMP2^-$) appeared flat with thin, well-extended actin fibers that traversed the cell, whereas those grown without doxycycline ($DOXY^-$/$rhBMP2^+$) showed increased actin at the plasma membrane with multiple cells also forming thickened actin stress fibers. When compared to cells grown on PB, cells on PSS_{28} appeared to grow more slowly. On PSS_{28}, doxycycline was without effect on actin fiber thickness or subcellular localization. However, cells in the $DOXY^-$/$rhBMP2^+$ cultures appeared larger than those in the $DOXY^+$/$rhBMP2^-$cultures.

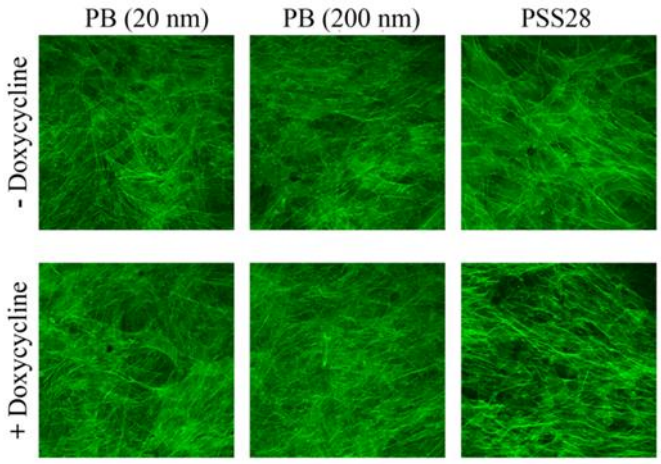

Figure 1. Confocal microscopy of C9 grown for four days on 20 nm thick polybutadiene (PB), on 200 nm thick PB, or on partially (28%) sulfonated polystyrene (PSS28) in the presence (+) or absence (−) of doxycycline and then fixed and labeled with AlexaFluor® 488-phalloidin to visualize f-actin.

rhBMP2-Induced Changes in Cell and Matrix Moduli: To determine whether C9 responds to the mechanics of PB, we measured the relative modulus of cells grown on 20 nm (thin) and 200 nm (thick) PB films where the moduli of the 20 nm PB film is 7-fold greater than that of the 200 nm film. The results are shown in Figure 2, where we can see that as early as the first day in culture, the moduli of the cells over-expressing rhBMP2 are larger than those of the cells where rhBMP2 expression is down regulated by DOXY. Furthermore, from the figure we can see the difference in moduli between cells plated on thin PB (hard) and thick PB (soft) substrates is nearly 50% for those expressing rhBMP2 vs. only 20% for those where expression is down-regulated. After three days in culture, the moduli of the cells expressing rhBMP2 decreases, but a significant differential between hard and soft substrates is maintained. On the other hand, for the cells where rhBMP2 expression is down-regulated, no change in modulus is observed, and the differential between the hard and soft substrates disappears completely. The importance of BMP2 in regulating osteogenic differentiation is well documented, but these results indicate that sensing substrate mechanics may be another important function in which it is implicated. The ability of cells to adjust their moduli to mimic that of their substrates had previously been discussed by Engler [30] within the context of preserving tensile integrity and leading to osteogenic differentiation in stem cells. This was further confirmed by Meng [36] who showed a direct correlation in MC3T3 cells between the early increase in cell modulus with eventual osteogenic differentiation and biomineral deposition after day 14. Hence, these results indicate that despite being a prominent osteogenic induction factor, the presence of rhBMP2, even when overexpressed, may not be sufficient to guarantee osteogenic differentiation. Rather, as previously discussed by Engler [30], the substrate modulus may also be an equally important factor.

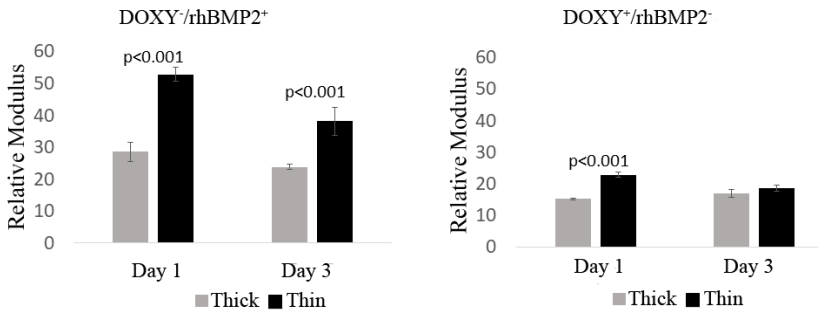

Figure 2. Comparison of relative moduli of C9 cells after 1- and 3-day incubation on 200 nm (gray) and 20 nm (black) PB films. **Left**: Cells overexpressing rhBMP2^{+}. **Right**: Cells where rhBMP2^{-} expression is suppressed.

The results for C9 cultured on PSS_{28} in the presence and absence of doxycycline are shown in Figure 3A. From the figure we can see that the moduli decrease after the first day, regardless of the addition of doxycycline or the level of rhBMP2. Hence, on this substrate doxycycline/rhBMP2 does not impact cell moduli during the first five days post-plating, although on day seven, the moduli of cells in the $DOXY^{-}$/$rhBMP2^{+}$ cultures increased while the modulus of the $DOXY^{+}$/$rhBMP2^{-}$ cells did not. It was previously shown that PSS_{28} surfaces support the formation of extracellular matrix fibers for multiple cell types [35,36]. We therefore also imaged the fibers (Figure 3B) and measured their moduli as a function of incubation time (Figure 3C). From the figures, we see that the morphology and the moduli of the fibrous matrices of the $DOXY^{-}$/$rhBMP2^{+}$ and $DOXY^{+}$/$rhBMP2^{-}$ cultures were similar and were greatest on day one and reduced by day three. A thin layer of the ECM proteins is also adsorbed in the interfiber spacing [35] but in a non-fibrous state. The interfiber moduli (Figure 3D) varied less and were 3-fold lower in both cultures on day one compared to their fibrous counterpart. This suggests that the cell moduli were mimicking that of the fibrous matrix proteins to which they adhered.

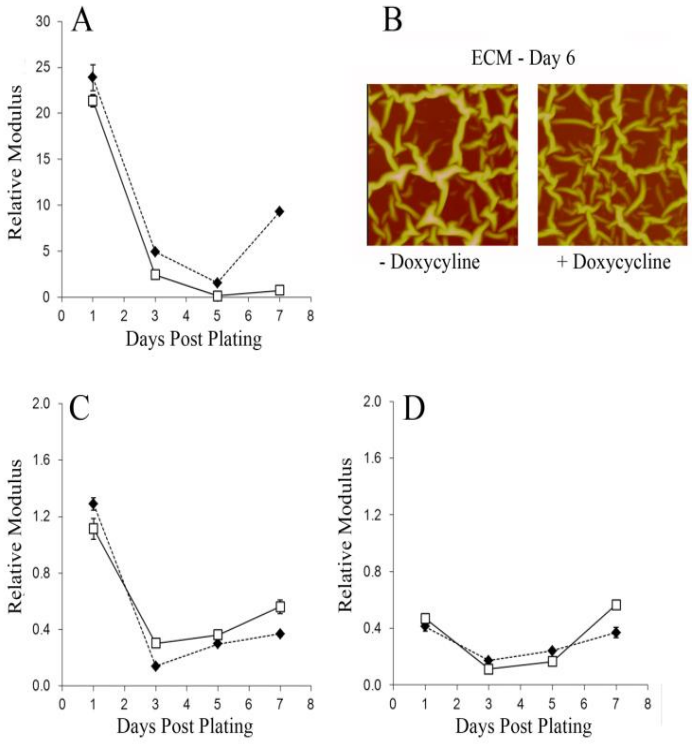

Figure 3. (**A**) Relative moduli of C9 cells plated on sulfonated PSS_{28} coated Si wafers with $DOXY^{-}$/$rhBMP2^{+}$ medium (filled circles) and $DOXY^{+}$/$rhBMP2^{-}$ (clear circles). (**B**) Topographical atomic force microscopy images of the extracellular matrix (ECM) fibers produced by the cells expressing (left) and not expressing BMP2 (right) after 6 days of incubation. Relative modulus of the ECM fibers (**C**) and interfiber spaces (**D**) are also shown.

Transcriptional Responses to rhBMP2 are Modified by Cell Substrates: The influence of the PB and PSS_{28} substrates on rhBMP2 expression and function were evaluated using qRT-PCR with primers to detect rhBMP2 and genes typically upregulated during chondrogenesis and endochondral bone formation: Aggrecan (ACAN), collagen X (COL X), osterix (OSX), and alkaline phosphatase (ALP) [39,40]. Aggrecan is the core cartilaginous protein glycosylated with chondroitin sulfate and keratan sulfate [41]. Collagen X is a matrix protein that is upregulated during chondrocyte hypertrophy [42] and osterix is a transcription factor required for endochondral bone formation [43–45] whose overexpression promotes the transcription of alkaline phosphatase [46]. As can be seen in Figure 4A, in media devoid of doxycycline, rhBMP2 was expressed in cells grown on all substrates (20 nm PB, 200 nm PB, and PSS_{28}) demonstrating maintenance of control by the Tetracycline Response Element independent

of surface. Similar to the expression pattern of rhBMP2, the steady state mRNA levels of osterix (Figure 4B), collagen X (Figure 4C), and alkaline phosphatase (Figure 4D) also increased in cultures grown without doxycycline. However, the rhBMP2-driven expression of aggrecan appeared limited to C9 cultured on the PB surfaces. The expression of aggrecan (Figure 4E) in cultures on PSS_{28} was not increased in the $DOXY^{-}/rhBMP2^{+}$ cultures. Although reduced aggrecan expression typifies both resting chondrocytes and mature hypertrophic chondrocytes [47], the co-expression of collagen X suggests a phenotype more closely approximating the hypertrophic chondrocyte.

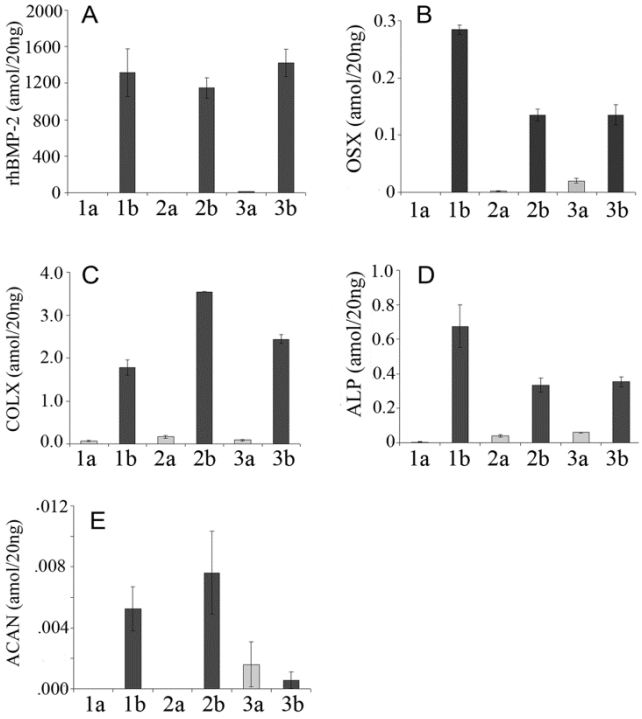

Figure 4. C9 was grown on 20 nm PB (1), 200 nm PB (2), or PSS_{28} (3) in $DOXY^{+}/rhBMP2^{-}$ medium (a) or $DOXY^{-}/rhBMP2^{+}$ medium (b) for 14 days. mRNA levels determined by qRT-PCR using primers for rhBMP2 (**A**), OSX (**B**), COL-X (**C**), ALP (**D**), and ACAN (**E**).

Substrate Control of Biomineralization Since hypertrophy is also linked to endochondral bone formation, we next analyzed biomineralization using cells grown for 14 days on spun cast films of PB and PSS_{28}. The 200 nm PB surfaces did not support mineralization by cell growth either with or without doxycycline. Similar results were obtained using the 20 nm PB surfaces. Only sporadic mineral deposits were found in in the $DOXY^{-}/rhBMP2^{+}$ cultures and none were observed in the $DOXY^{+}/rhBMP2^{-}$ cultures. In contrast, as can be seen in Figure 5, on PSS_{28} the $DOXY^{-}/rhBMP2^{+}$ cultures have a mineralized layer, nearly 1 µm thick, which by EDX contained calcium phosphate. The nature of the deposits was further confirmed by setting windows on the phosphorous, calcium, and silicon peaks in the EDX spectra and scanning the surface, where we can see that the layer is composed of hydroxyapatite, rather than calcium carbonate.

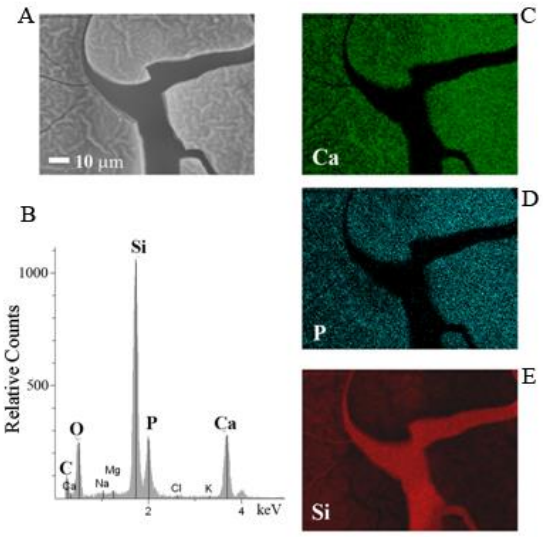

Figure 5. (**A**) SEM image of biomineralized film deposited by the C9 cells after 14 days in culture on PSS28, clearly showing the ECM fibers. (**B**) EDX spectra of the film showing the presence of Ca, P, O, and Si minerals present. (**C**–**E**) Elemental maps of Ca, P, and Si on the surface with overlap of Ca and P consistent with a uniform layer of hydroxyapatite incorporated into the ECM fibers shown in (**A**).

In order to determine the response of cells to a heterogeneous environment, mineralization was also assessed in cultures grown on spun cast films where the PB and PSS_{28} polymers were blended in a ratio of 1:1. Cultures on the nonblended polymers served as control. The topographical scans of PB, PSS_{28}, and the polymer blend film are shown in Figure 6A–C, respectively. From Figure 6C we can see that droplets of one phase rest on a flat layer of the other layer. The morphology of the film, obtained from analyzing Figure 6D, is illustrated in Figure 6K, where we see that a flat polymer layer, approximately 107 nm thick, coats the Si surface, while another polymer segregates to the air interface. Since the two polymers are highly immiscible, the polymers dewet with the upper layer forming droplets approximately 200 nm high, 0.5–1.5 microns in diameter, and with a contact angle exceeding 15°. From the lateral force image (Figure 6H), we find that the droplets are harder than the flat layer, which is consistent with the hydrophobic PB polymer segregating as a layer at the Si substrate, which was rendered hydrophobic prior to spin casting via HF etching. The PSS_{28} polymer, which is relatively hydrophilic, segregates away from the Si surface, but dewets the PB surface, which has a lower surface tension. Consequently, these samples provide surfaces with both chemical and topographical heterogeneity on a scale smaller than the area of a typical cell. SEM of the $DOXY^{-}$/$BMP\text{-}2^{+}$ cultures is shown in Figure 6E–G, where we see mineral deposits on both the PSS_{28} polymer and the polymer blend; no mineral deposits were detected on the PB surface. From the EDX we see that both the polymer (Figure 6I) and the polymer blend (Figure 6J) contain phosphorous, calcium, and oxygen consistent with deposition of calcium phosphate.

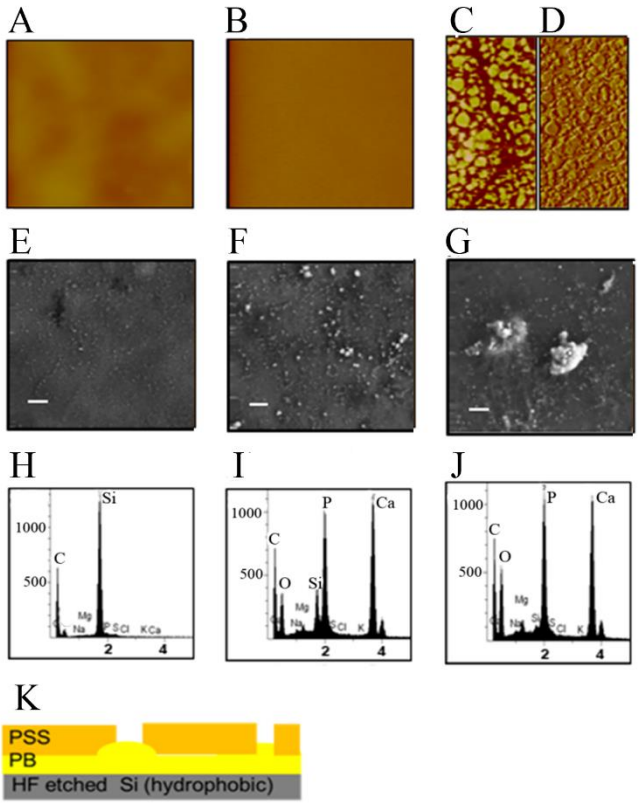

Figure 6. Atomic force microscopy images of polymer coatings spun cast on HF-etched Si with (**A**) 200 nm PB (**B**) 20 nm PSS28, and (**C**) a 1:1 binary PS28/PB blend. (**D**) Lateral force image corresponding to (**C**). Scanning electron microscope images of the films surfaces following incubation by the C9 expressing rhBMP-2: (**E**) 200 nm PB, (**F**) 20 nm PSS28, and (**G**) 1:1 binary PB/PSS28 blend. EDX spectra plotted as counts (y-axis) vs. energy (keV; x-axis) corresponding to the SEM images for (**H**) 200 nm PB, (**I**) 20 nm PSS_{28}, and (**J**) 1:1 Binary PSS28/PB blend. (**K**) Schematic of the polymers in the phase segregated blend film. The scale bar in panels **E**–**G** is 20 μm. Panels **A** and **B** are 20 μm × 20 μm, and Panel **C** and **D** are 20 μm × 10 μm.

In Figure 7A,B, we plot the relative moduli of the surfaces and of the cells grown on these surfaces. From Figure 7A we see that the modulus of the glassy PSS_{28} polymer is more than 300 times harder than that of the elastomeric liquid PB surface, while the modulus of the dewet PSS_{28} droplets coupled to the underlying PB layer is approximately 50 times larger. From Figure 7B we see that in the $DOXY^{+}/rhBMP2^{-}$ medium (light gray bars), the relative moduli of cells follows that of the surface where cells grown on the polymer blend and PSS_{28} homopolymer were more than 20 times and 90 times harder, respectively, than cells on PB. However, in $DOXY^{-}/rhBMP2^{+}$ medium, the relative cell moduli on both the polymer blend and PSS_{28} homopolymer appeared 80–100 fold greater than the modulus of cells on PB. To determine whether differentiation on the polymer blend is similar to the PSS_{28} or PB homopolymer, ACAN expression was measured. As we showed in Figure 4, the regulation of this gene differs from that of the other differentiation markers (ALP, OSX, and COL-X) tested. ALP, OSX, and COL-X expression are upregulated by rhBMP2 in cultures grown either on PB or on PSS_{28}. In contrast, ACAN expression is upregulated by rhBMP2 only in cultures grown on PB. As we see in Figure 7C, similar to the results on the PSS_{28} homopolymer, on the PB:PSS_{28} polymer blend, ACAN expression was not responsive to rhBMP2. In these experiments, ACAN expression on the polymer blend was detectable, while the level of expression in cultures on PSS_{28} was below the level of detection. Taken together the data support the conclusion that when cells are cultured on a polymer blend of PSS_{28}:PB, with microscale chemical heterogeneity smaller than the size of the cell, the cells will favor one surface over the other rather than having a mixed phenotype in culture.

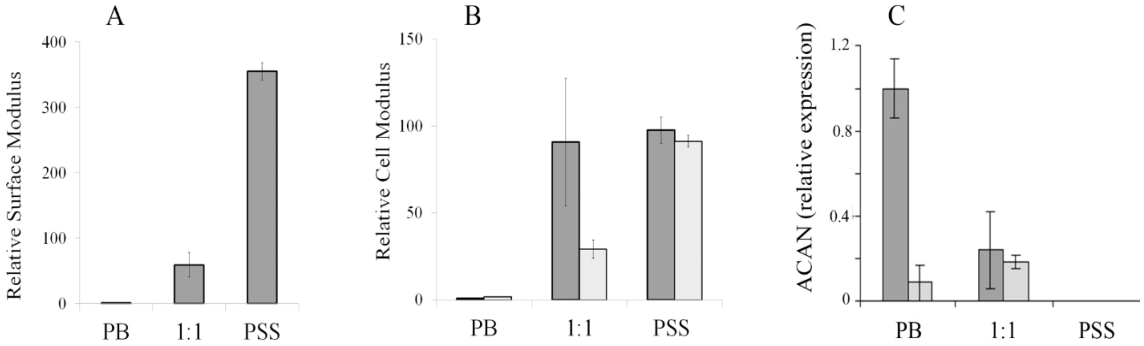

Figure 7. Scanning modulation force microscopy (SMFM) was carried out on (**A**) PB, PSS_{28}, and a 1:1 blend of PB and PSS_{28} (1:1) and on (**B**) live cells cultured on these substrates for 4 days in $DOXY^-/rhBMP2^+$ medium (dark gray bars) or $DOXY^+/rhBMP2^-$ medium (light gray bars). ACAN mRNA expression (**C**) was evaluated after 14 days of growth.

4. Conclusions

We have investigated how substrate mechanics and chemistry influence cell responses to cytokines using PB and PSS_{28} substrates and the mouse MSC line, C9. This cell line is genetically modified to express rhBMP2 under control of tetracycline (or its homologue doxycycline) and undergoes osteo/chondrogenesis in response to BMP2. The modulus of PB varied ~7-fold (1–7 MPa) by adjusting PB film thickness from 20 nm to 200 nm. In the absence of doxycycline ($rhBMP2^+$), cells were sensitive to substrate mechanics and showed ~2-fold higher moduli on the 20 nm PB surfaces compared to the 200 nm PB surfaces. No significant differences in moduli were detected in cells grown with doxycycline (rhBMP2-negative). Yet, at day 14 in culture, in the absence doxycycline ($rhBMP2^+$) independent of substrate modulus, cells showed increased expression of early differentiation markers (OSX and ALP) and markers unique to chondrogenesis (COL-X and ACAN). Mineralization was not observed with the exception of sporadic deposits on the 20 nm PB films in doxycycline-free cultures. On PSS_{28}, independent of doxycycline, cells had high moduli within 24 h of plating where the mechanical properties of the cells reflected that of the ECM rather than that of the substrate. Although cell and ECM moduli were not influenced by doxycycline, in its absence biomineral deposits were formed, and OSX, ALP, and COL-X expression increased. ACAN expression did not. This phenotype, unlike that of cells on PB, mimics that of the hypertrophic chondrocyte. Substrates were also prepared from PSS_{28}/PB blends, where the surfaces exhibited chemically heterogeneous morphologies. Cells plated on these substrates responded in the same manner as those plated on homogeneous PSS_{28} films, despite there being PB regions as well, indicating that the phenotype induced by the PSS_{28} is predominant. Taken together the data support the notion that substrate mechanics and chemistry can regulate cellular response to rhBMP2.

Author Contributions: Conceptualization & Formal analysis, A.B., G.P., Z.G., D.G., M.R. and M.S.; Data curation, C.C., M.R. and M.S.; Funding acquisition, M.R.; Investigation, A.B. and C.C.; Methodology, A.B., C.C., Z.G., D.G., and M.R.; Project administration, M.R. and M.S.; Resources, Z.G., D.G., M.R. and M.S.; Supervision, M.R. and M.S.; Writing—original draft, A.B., M.R. and M.S.; Writing—review & editing, A.B., G.P., Z.G., D.G., M.R. and M.S.

Funding: This work was supported in part by the National Science Foundation (Inspire Program Award number: 1344267).

Conflicts of Interest: The authors declare no conflicts of interest

References

1. Garrison, K.R.; Donell, S.; Ryder, J.; Shemilt, I.; Mugford, M.; Harvey, I.; Song, F. Clinical effectiveness and cost-effectiveness of bone morphogenetic proteins in the non-healing of fractures and spinal fusion: A systematic review. *Health Technol. Assess* **2007**, *11*, 1–150. [CrossRef] [PubMed]

2. Lissenberg-Thunnissen, S.N.; De Gorter, D.J.J.; Sier, C.F.M.; Schipper, I.B. Use and efficacy of bone morphogenetic proteins in fracture healing. *Int. Orthop.* **2011**, *35*, 1271–1280. [CrossRef] [PubMed]
3. Song, B.; Estrada, K.D.; Lyons, K.M. Smad signaling in skeletal development and regeneration. *Cytokine Growth Factor Rev.* **2009**, *20*, 379–388. [CrossRef]
4. Rosen, V. BMP2 signaling in bone development and repair. *Cytokine Growth Factor Rev.* **2009**, *20*, 475–480. [CrossRef]
5. Mi, M.; Jin, H.; Wang, B.; Yukata, K.; Sheu, T.-J.; Ke, Q.H.; Tong, P.; Im, H.-J.; Guozhi, X.; Chen, D. Chondrocyte BMP2 signaling plays an essential role in bone fracture healing. *Gene* **2013**, *512*, 211–218. [CrossRef] [PubMed]
6. Edgar, C.M.; Chakravarthy, V.; Barnes, G.; Kakar, S.; Gerstenfeld, L.C.; Einhorn, T.J. Autogenous regulation of a network of bone morphogenetic proteins (BMPs) mediates the osteogenic differentiation in murine marrow stromal cells. *Bone* **2009**, *40*, 1389–1398. [CrossRef] [PubMed]
7. Tsuji, K.; Bandyopadhyay, A.; Harfe, B.D.; Cox, K.; Kakar, S.; Gerstenfeld, L.; Einhorn, T.; Tabin, C.J.; Rosen, V. BMP2 activity, although dispensable for bone formation, is required for the initiation of fracture healing. *Nat. Genet.* **2006**, *38*, 1424. [CrossRef]
8. Wong, D.A.; Kumar, A.; Jatana, S.; Ghiselli, G.; Wong, K. Neurologic impairment from ectopic bone in the lumbar canal: A potential complication of off-label PLIF/TLIF use of bone morphogenetic protein-2 (BMP-2). *Spine J.* **2008**, *8*, 1011–1018. [CrossRef]
9. Kaneko, H.; Arakawa, T.; Mano, H.; Kaneda, T.; Kaneda, T.; Ogasawara, A.; Nakagawa, M.; Nakagawa, M.; Toyama, Y.; Yabe, Y.; et al. Direct stimulation of osteoclasticbone resorption by bone morphogenetic protein (BMP)-2 and expression of BMP receptors in mature osteoclasts. *Bone* **2000**, *27*, 479–486. [CrossRef]
10. Smucker, J.D.; Rhee, J.M.; Singh, K.; Yoon, S.T.; Heller, J.G. Increased swelling complications associated with off-label usage of rhBMP-2 in the anterior cervical spine. *Spine* **2006**, *31*, 2813–2819. [CrossRef]
11. Vaidya, R.; Weir, R.; Sethi, A.; Meisterling, S.; Hakeos, W.; Wybo, C.D. Interbody fusion with allograft and rhBMP-2 leads to consistent fusion but early subsidence. *J. Bone Jt. Surg. Br.* **2007**, *89*, 342–345. [CrossRef] [PubMed]
12. Zara, J.N.; Siu, R.K.; Zhang, X.; Shen, J.; Ngo, R.; Lee, M.; Li, W.; Chiang, M.; Chung, J.; Kwak, J.; et al. High doses of bone morphogenetic protein 2 induce structurally abnormal bone and inflammation in vivo. *Tissue Eng. Part A* **2011**, *17*, 1389–1399. [CrossRef] [PubMed]
13. Denker, A.E.; Haas, A.R.; Nicoll, S.B.; Tuan, R.S. Chondrogenic differentiation of murine C3H10T1/2 multipotential mesenchymal cells: I. Stimulation by bone morphogenetic protein-2 in high-density micromass cultures. *Differentiation* **1999**, *64*, 67–76. [CrossRef] [PubMed]
14. Hasharoni, A.; Zilberman, Y.; Turgeman, G.; Helm, G.A.; Liebergall, M.; Gazit, D. Murine spinal fusion induced by engineered mesenchymal stem cells that conditionally express bone morphogenetic protein-2. *J. Neurosurg. Spine.* **2005**, *3*, 47–52. [CrossRef] [PubMed]
15. Moutsatsos, I.K.; Turgeman, G.; Zhou, S.; Kurkalli, B.G.; Pelled, G.; Tzur, L.; Kelley, P.; Stumm, N.; Mi, S.; Müller, R.; et al. Exogenously regulated stem cell-mediated gene therapy for bone regeneration. *Mol. Ther.* **2001**, *3*, 449–461. [CrossRef] [PubMed]
16. Sheyn, D.; Ruthemann, M.; Mizrahi, O.; Kallai, I.; Zilberman, Y.; Tawackoli, W.; Kanim, L.E.; Zhao, L.; Bae, H.; Pelled, G.; et al. Genetically modified mesenchymal stem cells induce mechanically stable posterior spine fusion. *Tissue Eng. Part A* **2010**, *16*, 3679–3686. [CrossRef] [PubMed]
17. Noel, D.; Gazit, D.; Bouquet, C.; Apparailly, F.; Bony, C.; Plence, P.; Millet, V.; Turgeman, G.; Perricaudet, M.; Sany, J.; et al. Short-term BMP-2 expression is sufficient for in vivo osteochondral differentiation of mesenchymal stem cells. *Stem Cells* **2004**, *22*, 74–85. [CrossRef] [PubMed]
18. Jones, E.; Yang, X. Mesenchymal stem cells and bone regeneration: Current status. *Injury* **2011**, *42*, 562–568. [CrossRef]
19. Griffin, M.; Igbal, S.A.; Bayat, A. Exploring the application of mesenchymal stem cells in bone repair and regeneration. *J. Bone Jt. Surg. Britain.* **2011**, *93*, 427–434. [CrossRef]
20. Kim, S.S.; Park, S.M.; Jeon, O.; Choi, Y.C.; Kim, B.S. Poly(lactide-co-glycolide)/hydroxyapatite composite scaffolds for bone tissue engineering. *Biomaterials* **2006**, *27*, 1399–1409. [CrossRef]
21. Frohlich, M.; Grayson, W.L.; Wan, L.Q.; Marolt, D.; Drobnic, M.; Vunjak-Novakovic, G. Tissue engineered bone grafts: Biological requirements, tissue culture and clinical relevance. *Curr. Stem Cell Res. Ther.* **2008**, *3*, 254–264. [CrossRef] [PubMed]

22. Li, J.; Hong, J.; Zheng, Q.; Guo, X.; Lan, S.; Cui, F.; Pan, H.; Zou, Z.; Chen, C. Repair of rat cranial bone defects with nHAC/PLLA and BMP-2-related peptide or rhBMP-2. *J. Orthop. Res.* **2011**, *29*, 1745–1752. [CrossRef] [PubMed]
23. He, X.; Liu, Y.; Yuan, X.; Lu, L. Enhanced healing of rat calvarial defects with MSCs loaded on BMP-2 releasing chitosan/alginate/hydroxyapatite scaffolds. *PLoS ONE* **2014**, *9*, e104061. [CrossRef] [PubMed]
24. Wang, X.; Wang, Y.; Gou, W.; Lu, Q.; Peng, J.; Lu, S. Role of mesenchymal stem cells in bone regeneration and fracture repair: A review. *Int. Orthop.* **2012**, *37*, 2491–2498. [CrossRef]
25. Ingber, D.E. Mechanosensation through integrins: Cells act locally but think globally. *Proc. Natl. Acad. Sci. USA* **2003**, *100*, 1472–1474. [CrossRef] [PubMed]
26. MacQueen, L.; Sun, Y.; Simmons, C.A. Mesenchymal stem cell mechanobiology and emerging experimental platforms. *J. R. Soc. Interface* **2013**, *10*, 20130179. [CrossRef] [PubMed]
27. Discher, D.E.; Janmey, P.; Wang, Y.-L. Tissue cells feel and respond to the stiffness of their substrate. *Science* **2005**, *310*, 1139–1143. [CrossRef] [PubMed]
28. Discher, D.E.; Mooney, D.J.; Zandstra, P.W. Growth factors, matrices, and forces combine and control stem cells. *Science* **2009**, *324*, 1673–1677. [CrossRef]
29. Wang, Y.K.; Yu, X.; Cohen, D.M.; Wozniak, M.A.; Yang, M.T.; Gao, L.; Eyckmans, J.; Chen, C.S. Bone morphogenetic protein-2-induced signaling and osteogenesis is regulated by cell shape, RhoA/ROCK, and cytoskeletal tension. *Stem Cells Dev.* **2011**, *21*, 1176–1186. [CrossRef]
30. Engler, A.J.; Sen, S.; Sweeney, H.L.; Discher, D.E. Matrix elasticity directs stem cell lineage specification. *Cell* **2006**, *126*, 677–689. [CrossRef]
31. Reilly, G.C.; Engler, A.J. Intrinsic extracellular matrix properties regulate stem cell differentiation. *J. Biomech.* **2010**, *43*, 55–62. [CrossRef] [PubMed]
32. Chang, C.; Bherwani, A.; Simon, M.; Rafailovich, M.; Jurukovski, V. Entangled polymer surface confinement, an alternative method to control stem cell differentiation in the absence of chemical mediators. *Ann. Mater. Sci. Eng.* **2014**, *1*, 7.
33. Aranguren, M.I.; Macosko, C.W. Modulus of polybutadiene networks by hydrosilation crosslinking. *Macromolecules* **1988**, *21*, 2483–2491. [CrossRef]
34. Athanasiou, K.A.; Rosenwasser, M.P.; Buckwalter, J.A.; Malinin, T.I.; Mow, V.C. Intersecies comparisons of in situ intrinsic mechanical properties of distal femoral cartilage. *J. Orthop. Res.* **1991**, *9*, 330–340. [CrossRef] [PubMed]
35. Pernodet, N.; Rafailovich, M.; Sokolov, J.; Xu, D.; Yang, N.L.; McLeod, K. Fibronectin fibrillogenesis n sulfonated polystyrene surfaces. *J. Biomed. Mater. Res. A* **2003**, *64*, 684–692. [CrossRef] [PubMed]
36. Meng, Y.M.; Qin, Y.-X.; DiMasi, E.; Ba, X.; Rafailovich, M.; Pernodet, N. Biomineralization of a self-assembled ex.racellular matrix for bone tissue engineering. *Tissue Eng. Part A* **2009**, *15*, 355–366. [CrossRef] [PubMed]
37. Ge, S.; Pu, Y.; Zhang, W.; Rafailovich, M.; Sokolov, J. Shear modulation force microscopy study of near surface glass transition temperatures. *Phys. Rev. Lett.* **2000**, *85*, 2340–2343. [CrossRef] [PubMed]
38. Pu, Y.; Ge, S.; Rafailovich, M.; Sokolov, J.; Duan, Y.; Pearce, E.; Zaitsev, V.; Schwarz, S. Surface transitions by shear modulation force microscopy. *Langmuir* **2001**, *17*, 5865–5871. [CrossRef]
39. Yagi, K.; Tsuji, K.; Nifuji, A.; Shinomiya, K.; Nakashima, K.; DeCrombrugghe, B.; Noda, M. Bone morphogenetic protein-2 enhances osterix gene expression in chondrocytes. *J. Cell. Biochem.* **2003**, *88*, 1077–1083. [CrossRef]
40. Zuscik, M.J.; Hilton, M.J.; Zhang, X.; Chen, D.; O'Keefe, R.J. Regulation of chondrogenesis and chondrocyte differentiation by stress. *J. Clin. Investig.* **2008**, *118*, 429–438. [CrossRef]
41. Kiani, C.; Chen, L.; Wu, Y.J.; Yee, A.J.; Yang, B.B. Structure and function of aggrecan. *Cell Res.* **2002**, *12*, 19–32. [CrossRef] [PubMed]
42. Nurminskaya, M.; Linsenmayer, T.F. Identification and characterization of up-regulated genes during chondrocyte hypertrophy. *Dev. Dyn.* **1996**, *206*, 260–271. [CrossRef]
43. Nakashima, K.; Zhou, X.; Kunkel, G.; Zhang, Z.; Deng, J.M.; Behringer, R.R.; de Crombrugghe, B. The novel zinc finger-containing transcription factor osterix is required forosteoblast differentiation and bone formation. *Cell* **2002**, *108*, 17–29. [CrossRef]
44. Jing, J.; Hinton, R.J.; Jing, Y.; Liu, Y.; Zhou, X.; Feng, J.Q. Osterix couples chondrogenesis and osteogenesis in post-natal condylar growth. *J. Dent. Res.* **2014**, *93*, 1014–1021. [CrossRef]

45. Oh, J.H.; Park, S.Y.; de Crombrugghe, B.; Kim, J.E. Chondrocyte-specific ablation of Osterix leads to impaired endochondral ossification. *Biochem. Biophys. Res. Commun.* **2012**, *418*, 634–640. [CrossRef]
46. Matsubara, T.; Kida, K.; Yamaguchi, A.; Hata, K.; Ichida, F.; Meguro, H.; Aburatani, H.; Nishimura, R.; Yoneda, T. BMP2 regulates osterix through Msx2 and Runx2 during osteoblast differentiation. *J. Biol. Chem.* **2008**, *283*, 29119–29125. [CrossRef]
47. Domowicz, M.S.; Cortes, M.; Henry, J.G.; Schwartz, N.B. Aggrecan modulation of growth plate morphogenesis. *Dev. Biol.* **2009**, *329*, 242–257. [CrossRef]